

Interplay between the d - and π -electron systems in magnetic torque of the layered organic conductor κ -(BETS)₂Mn[N(CN)₂]₃

O. M. Vyaselev,^{1,*} W. Biberacher,² N. D. Kushch,³ and M. V. Kartsovnik^{2,†}¹*Institute of Solid State Physics, Russian Academy of Sciences, Academician Ossipyan str. 2, 142432 Chernogolovka, Moscow region, Russia*²*Walther-Meißner-Institut, Bayerische Akademie der Wissenschaften, Walther-Meißner-Str. 8, 85748 Garching, Germany*³*Institute of Problems of Chemical Physics, Russian Academy of Sciences, Academician Semenov ave. 1, 142432 Chernogolovka, Moscow region, Russia*

(Received 14 August 2017; revised manuscript received 31 October 2017; published 29 November 2017)

In the organic charge transfer salt κ -(BETS)₂Mn[N(CN)₂]₃ the metallic conductivity is provided by itinerant π electrons in the layers of BETS molecules, whereas magnetization is largely dominated by the localized d electrons of the Mn²⁺ ions in the insulating anionic layers. We study magnetic properties of the compound in its low-temperature, Mott-insulating state by means of magnetic torque technique. The complex behavior of the torque can be consistently explained by the coexistence of two weakly interacting magnetic subsystems associated with paramagnetic d -electron spins and antiferromagnetically ordered π -electron spins, respectively. Based on the experimental data, we determine the principal axes of magnetization of the Mn²⁺ sublattice and propose a qualitative model for the π -electron spin arrangement, implying an important role of the Dzyaloshinskii-Moriya interaction.

DOI: [10.1103/PhysRevB.96.205154](https://doi.org/10.1103/PhysRevB.96.205154)

I. INTRODUCTION

The organic radical cation salt κ -(BETS)₂Mn[N(CN)₂]₃, where BETS stands for bis-(ethylenedithio)-tetraselenafulvalene, has a layered structure consisting of conducting sheets of BETS donor molecules, sandwiched between insulating Mn[N(CN)₂]₃⁻ anion layers [1,2]. This compound adds to the series of BETS salts with spatially separated conducting and magnetic systems synthesized in a quest for hybrid multifunctional molecular materials combining conducting and magnetic properties in the same crystal lattice, potentially promising for microelectronics. The earlier members of this family, λ - and κ -(BETS)₂FeX₄ (X = Cl, Br) [3–6], have been of strong interest due to prominent interactions between the localized d -electron spins of the Fe³⁺ ions in the insulating layers and itinerant π electrons in the conducting BETS layers. For example, a considerable π - d coupling in λ -(BETS)₂FeCl₄ leads to a metal-insulator transition in the π -electron system triggered by an antiferromagnetic (AF) ordering of localized Fe³⁺ spins [7] and to a spectacular phenomenon of superconductivity induced by a strong magnetic field [8,9]. In the κ -(BETS)₂FeX₄ salts the π - d coupling is weaker; however it can be readily traced in a reconstruction of the Fermi surface caused in the AF state [10–12], high-field reentrant superconductivity [13,14], and protection of the low-field superconductivity by the AF ordering [13,15].

In the present compound the π - d interactions seem to be even weaker. While the metal-insulator transition at $T_{MI} \approx 21$ K [1] might, at first glance, appear similar to that in λ -(BETS)₂FeCl₄, it is most likely driven by purely the Mott-insulating instability of the π -electron system and not by an AF instability of the localized d -electron spins. Indeed, clear indications of a long-range AF ordering of the itinerant π -electron spins have been obtained in NMR experiments

at $T < T_{MI}$ [16,17], whereas no sign for a long-range order was found for the Mn²⁺ subsystem [18,19]. Several anomalies associated with the metal-insulator transition have also been found in magnetic torque experiments [1,18]. However, their exact origin has been not clarified yet. Here we present a comprehensive study of magnetic torque in the insulating state of κ -(BETS)₂Mn[N(CN)₂]₃ and discuss its behavior taking into account the coexistence of the two weakly interacting spin subsystems.

The paper is organized as follows. The information on the crystal structure of κ -(BETS)₂Mn[N(CN)₂]₃ and on the experimental technique is given in Sec. II. In Sec. III the field-dependent magnetic torque measured at different orientations of magnetic field rotated in four planes perpendicular to the conducting layers are presented and several important distinctive features of its behavior are outlined. Section IV, divided into four parts (A to D), is devoted to the analysis of the experimental results in terms of separate contributions of two spin subsystems and a weak interaction between the latter. It starts with introducing general expressions for the magnetic torque on an anisotropic paramagnet, which describe the main contribution, coming from the d -electron spins of Mn²⁺, in the low- ($\lesssim 2$ T) and high-field ($\gtrsim 10$ T) regimes. In Sec. IV B we propose a procedure for analyzing the torque experienced by a saturated anisotropic paramagnet, which allows us to determine the principal magnetization axes of Mn²⁺ spin subsystem at high fields. While the smooth field dependence of the torque is strongly dominated by Mn²⁺, the AF ordered π electrons clearly manifest themselves in a steplike anomaly, which is attributed to a field-induced spin reorientation transition in this subsystem. In Sec. IV C we examine the angular dependence of this anomaly and propose a scheme of the canted AF spin arrangement below and above the spin-reorientation transition. Section IV D addresses the interaction between the two spin subsystem as it shows up in the nonmonotonic field dependence of the torque at intermediate fields. Finally, Sec. V summarizes the main results obtained in this work.

*vyasel@issp.ac.ru

†mark.kartsovnik@wmi.badw-muenchen.de

II. EXPERIMENT

The crystal structure of κ -(BETS)₂Mn[N(CN)₂]₃ is monoclinic; the space group is $P2_1/c$ and the lattice constants at 15 K are $a = 19.421 \text{ \AA}$, $b = 8.346 \text{ \AA}$, $c = 11.830 \text{ \AA}$, $\beta = 92.90^\circ$, $V = 1915.0 \text{ \AA}^3$, and $\rho = 2.424 \text{ g/cm}^3$, with two formula units per unit cell [2]. The conducting layers are formed by BETS dimers in the bc plane and sandwiched between the polymeric $\text{Mn}[\text{N}(\text{CN})_2]_3^-$ anion layers in the a direction. The crystal growth procedure and details of the structure have been reported elsewhere [1,2]. Results of the magnetization measurements have been reported previously [18].

The sample was a $40 \mu\text{g}$ thin-plate single crystal of $\sim 0.7 \times 0.3 \times 0.08 \text{ mm}^3$ size, with the largest dimensions along the conducting BETS layers (crystallographic bc plane). Magnetic torque was measured in fields up to 15 T with a homemade cantilever beam torquemeter described in [20]. The cantilever was made of $50 \mu\text{m}$ thick as-rolled beryllium-copper foil. The torque was determined from the change of the capacitance between the cantilever disk, to which the sample is attached, and the ground plate. The capacitance was measured using a tunable capacitance bridge. The maximum torque of the cantilever produced by the gravity force (in zero applied field) was $1.16 \times 10^{-7} \text{ N m}$, this value was used to convert the measured changes in capacitance to the units of torque. The torquemeter was attached to a rotation stage whose rotation axis was perpendicular to both the external magnetic field and the working plane of the cantilever. In this geometry, the component of the torque along the rotation axis is measured.

III. RESULTS

Figures 1(a)–1(d) show the magnetic field dependence of the torque $\tau(H)$ on the κ -(BETS)₂Mn[N(CN)₂]₃ crystal measured at 1.5 K, with the rotation axis parallel, respectively, to $[0\bar{1}0]$ (τ_b), $[001]$ (τ_c), $[0\bar{1}1]$ (τ_d), and perpendicular to $[0\bar{1}1]$ in the bc plane ($\tau_{\perp d}$). Numbers to the right of the curves indicate the polar angle θ between the field direction and a^* , the direction perpendicular to the crystallographic (bc) plane.

There are several notable features in Fig. 1, which will be discussed below:

(i) At high fields ($\mu_0 H > 10 \text{ T}$) the torque becomes constant in field.

(ii) For the angles where the high-field torque is small, see, e.g., the $\theta = 22^\circ$ curve for τ_b in Fig. 1(a) or the $\theta = -6^\circ$ curve for τ_c in Fig. 1(b), the torque is nonmonotonic in the range between $\simeq 2.5$ and 7.5 T .

(iii) At some angles τ_c , τ_d , and $\tau_{\perp d}$ demonstrate a steplike feature (“kink”) at fields 7–10 T. Figure 2 shows the kinks in more details. No such kinks have been detected for τ_b at any θ .

Features (ii) and (iii) vanish as the temperature is increased above T_{MI} : the kinks disappear [18], the field dependence becomes monotonic and gradually acquires the simple parabolic form usual for an anisotropic paramagnet at $\mu_B B \ll k_B T$ (where μ_B is the Bohr magneton and k_B is the Boltzmann constant). Therefore, these features must be associated with the low-temperature insulating state with antiferromagnetically ordered π -electron spins.

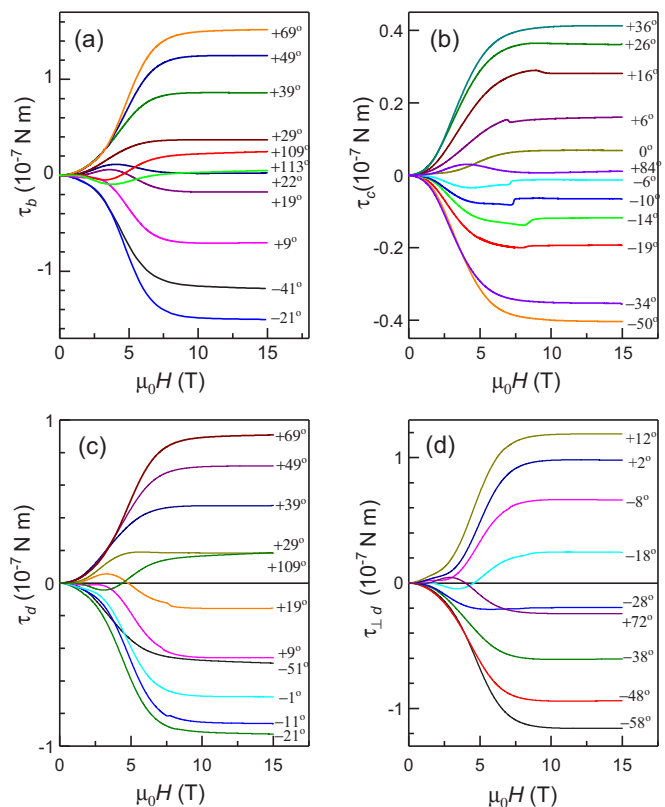


FIG. 1. Field dependence of the magnetic torque of κ -(BETS)₂Mn[N(CN)₂]₃ measured at $T = 1.5 \text{ K}$ for the rotation axis parallel to directions: (a) $[0\bar{1}0]$, (b) $[001]$, (c) $[0\bar{1}1]$, and (d) perpendicular to $[0\bar{1}1]$ in the bc plane. Numbers to the right of the curves indicate the polar angle θ between the field direction and a^* , the normal to the crystallographic bc plane.

On the other hand, the field directions where the high-field torque is zero $\mu_0 H = 15 \text{ T}$, e.g., $\theta \simeq 22^\circ \pm 90^\circ$ for τ_b [Fig. 1(a)] or $\theta \simeq -6^\circ \pm 90^\circ$ for τ_c [Fig. 1(b)], are at $T = 1.5 \text{ K}$, the same as at high temperatures ($T > T_{\text{MI}}$) within the

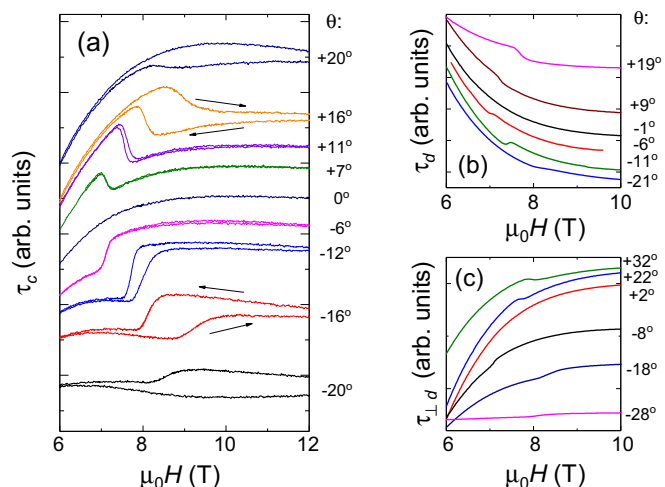


FIG. 2. A closeup of the steplike features (kinks) in the H dependence of τ_c (a), τ_d (b), and $\tau_{\perp d}$ (c). The curves are shifted along the vertical axis for clarity.

experimental accuracy $\pm 0.5^\circ$. This means that the principal axes of the high-field magnetization above and below T_M coincide.

IV. DISCUSSION

The absolute values of torque in Fig. 1 are more than an order of magnitude higher than in the structurally similar but free of magnetic ions charge-transfer salt κ -(BEDT-TTF)₂Cu[N(CN)₂]Cl [21]. In turn, the kinks have been related to the antiferromagnetically ordered π -electron spins [18]. In what follows we characterize the phenomena associated with each spin subsystem separately and address implications of their interaction.

A. General expressions for the magnetic torque

The magnetic torque is expressed as

$$\boldsymbol{\tau} = V \mathbf{M} \times \mathbf{B}, \quad (1)$$

where V is the volume of the sample, \mathbf{M} is the sample magnetization, and $\mathbf{B} = \mu_0 \mathbf{H} + \mu_0 \mathbf{M}$ is the magnetic field. Let us neglect for a while the ramifications due to the sample shape (that will be discussed below) and assume the sample is a sphere. In that case

$$\boldsymbol{\tau} = V \mu_0 \mathbf{M} \times (\mathbf{H} + \mathbf{M}) = V \mu_0 \mathbf{M} \times \mathbf{H}. \quad (2)$$

Consider first the high-temperature, low-field limit, $\mu_B B \ll k_B T$. Assuming the field in the (XY) plane where X and Y are the magnetization principal axes,

$$\mathbf{H} = H[\cos \theta, \sin \theta, 0], \quad (3)$$

and the susceptibility tensor

$$\hat{\chi} = \begin{pmatrix} \chi_X & 0 & 0 \\ 0 & \chi_Y & 0 \\ 0 & 0 & \chi_Z \end{pmatrix}, \quad (4)$$

one obtains the magnetization

$$\mathbf{M} = \hat{\chi} \cdot \mathbf{H} = H[\chi_X \cos \theta, \chi_Y \sin \theta, 0], \quad (5)$$

and the torque $\boldsymbol{\tau} = V \mathbf{M} \times \mathbf{H} = [0, 0, \tau_Z]$, where

$$\tau_Z = \frac{1}{2} V H^2 (\chi_X - \chi_Y) \sin 2\theta, \quad (6)$$

which gives a quadratic in H behavior of the torque at low fields/high temperatures, consistent with the experiment at $\mu_0 H < 2$ T, see Fig. 1.

In the high-field, low-temperature regime, $\mu_B H \gg k_B T$, the linear field dependence given by Eq. (5) is no longer valid. The magnetization of a paramagnet saturates, and in a system with an isotropic g factor, the effect of changing H reduces to a change of the angle between the magnetization vector and the field direction. In that case the axial anisotropy follows a H^{-2} law [22], so that at $H \rightarrow \infty$ the torque asymptotically approaches a constant value modulated by a $\sin 2\theta$ angular dependence. This behavior of the torque is indeed observed in our experiment, as is seen in Fig. 1 for $\mu_0 H > 10$ T.

However, the nonmonotonic field dependence of torque observed in the range 2.5–7.5 T and the kink features cannot be described within the model of an anisotropic paramagnet but

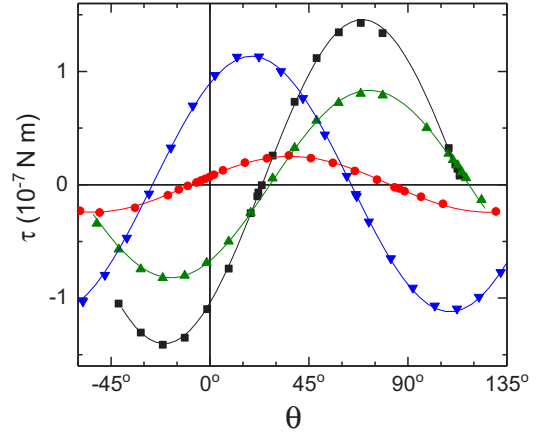


FIG. 3. Angular dependence of the torque at 1.5 K, 15 T for the field rotated around $[0\bar{1}0]$ (squares), $[001]$ (circles), $[0\bar{1}1]$ (up-triangles), and perpendicular to $[0\bar{1}1]$ in the bc plane (down-triangles). Solid lines: Fits to the data using Eq. (7).

arise apparently due to the AF-ordered spins of the π -electron subsystem, as discussed below.

B. Principal axes of magnetization

We now proceed to determining directions of the principal axes of the magnetization in κ -(BETS)₂Mn[N(CN)₂]₃.

Figure 3 shows the angle-dependent torque for different rotations at $T = 1.5$ K, $\mu_0 H = 15$ T. The raw experimental data have been corrected for the demagnetization effect as explained in the Appendix.

As one can see in Fig. 3, all four curves follow nicely the dependence: $\tau = \tau_{\max} \sin 2(\theta - \theta_0)$ with the parameters τ_{\max} and θ_0 listed in Table I. For the practical reasons which will become clear below, it is more convenient to present this dependence in the form

$$\tau = \alpha \cos 2\theta + \beta \sin 2\theta, \quad (7)$$

where $\alpha = -\tau_{\max} \sin 2\theta_0$ and $\beta = \tau_{\max} \cos 2\theta_0$.

In order to analyze the experimental results, we introduce the coordinate system $\{x, y, z\}$, where x is parallel to a^* while y and z coincide with crystallographic b and c axes, respectively. The rotation axis vector is given by $\mathbf{R} = [0, -\cos \phi, \sin \phi]$, where ϕ is the angle between the rotation axis and the $-\mathbf{b}$ direction. The values of ϕ for the four reported rotations are listed in Table I.

As mentioned above, at high field the linearity between \mathbf{M} and \mathbf{H} in the form of Eq. (5) is no longer valid. In order to calculate the magnetization direction in this case, instead of the susceptibility tensor $\hat{\chi}$ we introduce tensor $\hat{\xi}$ of the directional

TABLE I. Fit parameters to the torque data in Fig. 3.

Rotation axis	ϕ	τ_{\max} (10^{-7} N m)	θ_0	α (10^{-7} N m)	β (10^{-7} N m)
$[0\bar{1}0]$	0	1.43	24°	-1.07	0.948
$[001]$	90°	0.246	-8.4°	0.071	0.236
$[0\bar{1}1]$	55°	0.827	27.5°	-0.678	0.474
$\perp [0\bar{1}1]$	145°	1.128	-26°	0.888	0.696

cosines between \mathbf{M} and \mathbf{H} vectors,

$$\hat{\xi} = \begin{pmatrix} d_{xy} + d_{xz} + d_{yz} & \xi_{xy} & \xi_{xz} \\ \xi_{xy} & -(d_{xy} - d_{xz}) + d_{yz} & \xi_{yz} \\ \xi_{xz} & \xi_{yz} & d_{xy} - d_{xz} + d_{yz} \end{pmatrix}, \quad (8)$$

where $d_{xy} = \xi_{xx} - \xi_{yy}$, $d_{xz} = \xi_{xx} - \xi_{zz}$, $d_{yz} = \xi_{yy} + \xi_{zz}$. In that case $\mathbf{M} = M\hat{\xi} \cdot \mathbf{h}$, where $\mathbf{h} = [\cos\theta, \sin\theta \sin\phi, \sin\theta \cos\phi]$ is the applied field unit vector. In the $H \rightarrow \infty$ limit \mathbf{M} aligns with \mathbf{H} , so that $(\hat{\xi} \cdot \mathbf{h}) \cdot \mathbf{h} = 1$. Then, since the torque at high field is known to have a $K \sin 2\theta$ dependence where K is a constant [22], instead of using Eq. (2) we express the torque as

$$\boldsymbol{\tau} = K/M(\mathbf{M} \times \mathbf{h}) = K(\hat{\xi} \cdot \mathbf{h}) \times \mathbf{h}. \quad (9)$$

The torque component along the rotation axis, which is measured in the experiment, is

$$\tau_\phi = \boldsymbol{\tau} \cdot \mathbf{R} = K\{-\cos 2\theta[\xi_{xz} \cos\phi + \xi_{xy} \sin\phi] + \sin 2\theta[d_{xy} + d_{xz} - (d_{xy} - d_{xz}) \cos 2\phi - \xi_{yz} \sin 2\phi]/2\}. \quad (10)$$

For the four rotation axes used in the experiment we obtain

$$\tau_b(\phi = 0) = K\{-\xi_{xz} \cos 2\theta + d_{xz} \sin 2\theta\}, \quad (11a)$$

$$\tau_c(\phi = 90^\circ) = K\{-\xi_{xy} \cos 2\theta + d_{xy} \sin 2\theta\}, \quad (11b)$$

$$\begin{aligned} \tau_d(\phi = 55^\circ) = K\{ & -(0.82\xi_{xy} + 0.57\xi_{xz}) \cos 2\theta \\ & + (0.67d_{xy} + 0.33d_{xz} - 0.47\xi_{yz}) \sin 2\theta\}, \end{aligned} \quad (11c)$$

$$\begin{aligned} \tau_{\perp d}(\phi = 145^\circ) = K\{ & -(-0.82\xi_{xz} + 0.57\xi_{xy}) \cos 2\theta \\ & + (0.33d_{xy} + 0.67d_{xz} + 0.47\xi_{yz}) \sin 2\theta\}. \end{aligned} \quad (11d)$$

In fact, a detailed inspection of the sample orientation for the c -axis rotation has revealed that the real direction of c axis was slightly (by $\sim 4^\circ$) tilted from the direction of the rotation axis, and the correct value for ϕ was 94° . Taking this into account, we obtain the corrected value for τ_c :

$$\begin{aligned} \tau_c(\phi = 94^\circ) = K\{ & -(0.998\xi_{xy} - 0.07\xi_{xz}) \cos 2\theta \\ & + (0.995d_{xy} + 0.005d_{xz} + 0.07\xi_{yz}) \sin 2\theta\}. \end{aligned} \quad (11e)$$

Equating the fit parameters α and β listed in Table I to the corresponding coefficients of $\cos 2\theta$ and $\sin 2\theta$ in Eq. (11), one obtains the matrix

$$K\hat{\xi} = \begin{pmatrix} 1.184 + Kd_{yz} & 0 & 1.07 \\ 0 & 0.712 + Kd_{yz} & 0 \\ 1.07 & 0 & -0.712 + Kd_{yz} \end{pmatrix}. \quad (12)$$

The magnetization principal axes are the eigenvectors of this matrix: $X = [\cos\theta_M, 0, \sin\theta_M]$; $Y = [0, 1, 0]$, $Z = [-\sin\theta_M, 0, \cos\theta_M]$ with $\theta_M = 24.2^\circ$ for any arbitrary d_{yz} . The xz plane of the magnetization principal axes coincides with the ac plane of the crystal, which is quite reasonable

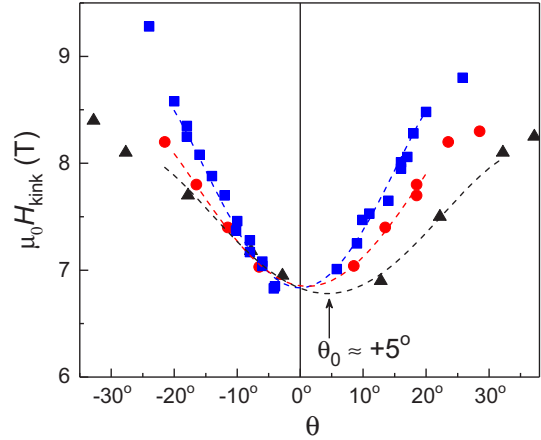


FIG. 4. Angle dependence of the position of the kink feature in the field-dependent torque τ_c (squares), τ_d (circles), and $\tau_{\perp d}$ (triangles).

since it is the mirror plane of the crystal structure. The X vector is directed at 24° from the a^* direction in the ac plane.

As it was mentioned above, at high temperatures the directions of the field where the torque vanishes, are the same as at $T = 1.5$ K, $\mu_0 H = 15$ T (Fig. 3). This implies that the obtained orientations of the principal axes of the magnetization are inherent to the Mn^{2+} spin system and do not change at the metal-insulator transition.

C. Angular and field dependence of the kinks

As one can see in Figs. 1 and 2, the kink feature in the torque exists when the field is tilted at a moderate angle $|\theta| \lesssim 30^\circ$ from the a^* direction around the axis parallel to crystallographic directions $[001]$ or $[0\bar{1}1]$ or perpendicular to $[0\bar{1}1]$, but not around the b axis ($[0\bar{1}0]$). Figure 4 shows the dependence of the kink position H_{kink} on the polar angle θ for the three above-mentioned rotation axes.

Thus, the following conditions should be satisfied in order to observe the kink:

- (1) there must be a sufficiently large field component along a^* ;
- (2) there must be a component of the field along $[010]$ (the b axis);
- (3) as mentioned above, the temperature must be below T_{MI} .

A very detailed description of the spin arrangement and field-induced spin reorientation (SR) transition in another Mott-insulating organic salt, κ -(BEDT-TTF) $_2$ Cu[N(CN) $_2$]Cl, which has a structure similar to the present compound and undergoes an AF transition below $T_N = 27$ K, has been given in [23,24]. The key concept is that in an AF system with a low symmetry of the underlying crystal structure, the two magnetic sublattices \mathbf{M}_1 and \mathbf{M}_2 do not arrange strictly antiparallel along the easy axis but form a *canted* antiferromagnetic (CAF) order due to the Dzyaloshinskii-Moriya (DM) interaction [25,26]. Following the notations of Ref. [24], we introduce the ferromagnetic and staggered magnetization vectors, which are expressed through the magnetization vectors of the magnetic sublattices as $\mathbf{M}_F = (\mathbf{M}_1 + \mathbf{M}_2)/2$ and $\mathbf{M}_S = (\mathbf{M}_1 - \mathbf{M}_2)/2$, respectively, see Fig. 5.

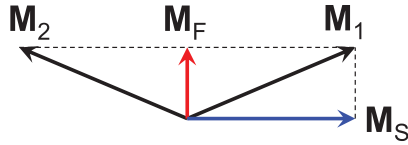


FIG. 5. Presentation of the (M_1, M_2) sublattice moments in the basis of ferromagnetic M_F and staggered M_S magnetization vectors.

The free energy of the CAF-ordered π -electron spin subsystem with the sublattice magnetizations outlined in Fig. 5, in the presence of the magnetic field, is composed of the Zeeman energy

$$E_Z = -(M_1 + M_2) \cdot H = -2M_F \cdot H, \quad (13)$$

the isotropic exchange energy

$$E_i = 2A(M_1 \cdot M_2) = 2A[(M_F)^2 - (M_S)^2], \quad (14)$$

the anisotropic exchange energy

$$E_a = 2K_a(M_1 \cdot k)(M_2 \cdot k) = 2K_a[(M_F \cdot k)^2 - (M_S \cdot k)^2], \quad (15)$$

and the DM term

$$E_{DM} = D \cdot (M_1 \times M) = 2D(M_F \times M_S), \quad (16)$$

where A and K_a are, respectively, the isotropic and anisotropic exchange constants, k is the unit vector along the anisotropic exchange easy axis, and D is the DM vector. E_z is minimized when $M_F \parallel H$, and E_i when $M_1 = M_2$, i.e., when $|M_F| = 0$, $|M_S| = M$ (M is the magnitude of the electron spin moment in both sublattices): the spins minimize E_i by aligning in an antiparallel orientation. E_a is minimum when $M_S \parallel k$ because $|E_a| \ll |E_i|$, hence $M_F \ll M_S$ [23,27], and the effect of E_{DM} is to arrange M_F and M_S perpendicular to D . The ultimate spin orientation is determined by a tradeoff between the four contributions to the total free energy.

The crystallographic ac plane is the mirror plane in the structure of κ -(BETS)₂Mn[N(CN)₂]₃. Symmetry considerations, thus, require k and D vectors to lie in the ac plane and M_F along the b axis. Recent calculations [28] have shown that the preferable orientation of vector D is the long axis of the BETS molecule, which is in our case directed at $\simeq 21^\circ$ from a^* in the ac plane. The exact direction of k is currently unknown. The overall easy axis k_S of the CAF-ordered π -spin subsystem is the compromise between the normal to vector D and the k direction.

Based on these considerations, one can propose a scheme of the SR transition responsible for the kink feature in the field-dependent torque. At zero field the AF sublattice moments are arranged as follows: M_F is along the b axis and $M_S \parallel k_S$ in the ac plane at some angle from D , as shown in Fig. 6(a).

As the magnetic field is applied with a strong enough component along M_S , so that $|E_z| > |E_a|$, the orientation of M_F along the b axis becomes unfavorable and it switches to (or maybe close to) the direction of the external field, producing an abrupt change in the magnetization anisotropy, hence a kink in the torque signal. In turn, M_S switches to the direction perpendicular to both M_F and D , see Fig. 6(b). Obviously, the minimum in H_{kink} should correspond to the external field

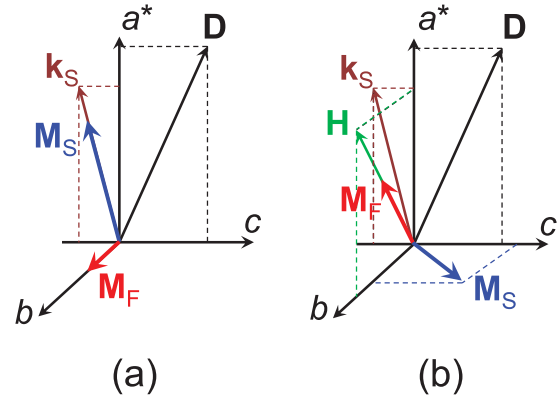


FIG. 6. Arrangement of the AF sublattice moments: (a) at zero field and (b) above the critical field of the SR transition H_{kink} .

direction along k_S . The experimental data on the angular dependence $H_{\text{kink}}(\theta)$ for different rotation planes shown in Fig. 4 give a key to understanding the orientation of k_S in the ac plane. One can notice that for the rotations around the c axis and $[0\bar{1}1]$ direction, H_{kink} is symmetric around $\theta = 0^\circ$, while for the rotation around the direction perpendicular to $[0\bar{1}1]$, which corresponds to the rotation plane closest to the ac plane, the minimum in $H_{\text{kink}}(\theta)$ is shifted by $\theta \approx 5^\circ$ from the a^* direction. For this rotation plane the projection of the field, applied at polar angle $\theta = 5^\circ$, on the ac plane makes an angle of $\approx 4^\circ$ with a^* . Therefore, it is likely that k_S is at some small angle from a^* in the $(a, -c)$ quadrant, as shown schematically in Fig. 6.

The suggested model of the AF spin arrangement explains the existence of the kinks in the field dependence of the measured torque, but does not explain why the kinks are only observed when the external field has a nonzero b -axis component. For example, no kink is found for the fields exactly perpendicular to the layers $\theta = 0^\circ$. One might doubt the existence of the SR transition at this field orientation. However, recent ¹³C NMR experiments confirm that it does exist [29]: in these experiments performed on a ¹³C-enriched crystal, the mentioned SR transition at $T < T_{\text{MI}}$ is seen as a dramatic change in the spectrum shape right at the same values and orientations of the magnetic field at which the kink in the field-dependent torque is observed, but also at $H \parallel a^*$ at $H \simeq 7$ T.

The apparent controversy can be resolved by taking into account that ac is the mirror plane of the crystal structure. Indeed, in this case the alignment of M_F along the b and $-b$ directions is equally favorable in the absence of external field. Therefore one can expect a domain structure to be formed with an equal number of the ferromagnetic moments M_F pointing to the directions b and $-b$, respectively. When an external field exceeding the critical value is applied exactly along the a^* direction ($\theta = 0^\circ$), the SR transition does occur, but the change in the torque caused by switching of M_F from the b direction to the external field direction is compensated by the same process in the domains where the zero-field moment M_F is pointing along $-b$. As a result no significant change in the total torque happens at such field orientation. By contrast, a nonzero b component of the applied field lifts this degeneracy, and the SR transition leads to a sizable step in the total torque.

D. Interaction between π - and d -spin subsystems

So far we considered the torque features caused by the d - and π -spin subsystems individually. In fact, the possibility to distinguish the contributions to the torque from the two subsystems indicates the weakness of π - d interactions, unlike, for example in λ -(BETS)₂FeCl₄, where both π - and d -electron spins are antiferromagnetically ordered [30,31] and their individual contributions to the torque can hardly be separated.

In κ -(BETS)₂Mn[N(CN)₂]₃, the π - d interaction between the essentially paramagnetic Mn²⁺ d -electron spin subsystem and the AF π -electron spin subsystem is apparently manifested in the nonmonotonic behavior of the torque in the intermediate field range, below $\simeq 7.5$ T for the directions of the field close to the magnetization principal axes (Fig. 1), at which the high-field/high-temperature torque is zero.

An isolated Mn²⁺ spin subsystem would produce a zero torque once the field is along any principal axis of the magnetization, since in that case the magnetization vector coincides with the field direction. However, at temperatures below T_{MI} π -electron spins form a long-range CAF order. Due to a finite ferromagnetic component M_F of the ordered π -electron moments, the d -electron spins experience a local exchange field caused by the π - d interaction. This gives rise to their nonzero magnetization even in the absence of the external field $\mathbf{H}_{\pi d}$. The orientation of the zero-field magnetization of Mn²⁺ depends on details of the π - d coupling and does not need to coincide with the directions of the magnetization principal axes. Therefore, in a small external field \mathbf{H} , even if it is applied along a principal axis, the magnetization of the Mn²⁺ subsystem is determined by the effective field $\mathbf{H}_{\text{eff}} = \mathbf{H} + \mathbf{H}_{\pi d}$, giving rise to a finite torque. As the external field (along the principal axis) increases, the Zeeman energy gradually overcomes the contribution from the π - d exchange, the magnetization vector turns towards the direction of \mathbf{H} , and the torque signal approaches zero. In our experiment this happens at $\simeq 7.5$ T, as one can see from Fig. 1. Thus, the observed nonmonotonic torque behavior can be understood as a result of the π - d exchange in κ -(BETS)₂Mn[N(CN)₂]₃. Yet other manifestations of the interaction between the two spin subsystems in this material are the violation of the Curie-Weiss behavior of the bulk magnetization [1,18] and a sharp increase of ¹H NMR linewidth [18,19] observed at $T < T_{\text{MI}}$.

The fact that below T_{MI} the AF-ordered π -spin subsystem does not induce the AF order in the d -electron Mn²⁺ spin subsystem has two origins. The first one is the weakness of π - d coupling. While the exact value of the exchange energy is unknown as yet, we can make an upper limit estimation. The absence of beats in the Shubnikov–de Haas effect in the interval 11 to 29 T [32] sets the upper limit for the effective internal field, imposed by the d -electron spins on the π -electron system [33,34]: $H_e = 4F_{\text{beat}}/(gm_c) < 2.5$ T, where the beat frequency $F_{\text{beat}} < 8.9$ T, $g \approx 2$ is the g factor, and $m_c = 7.0$ is the relevant effective cyclotron mass in units of the free electron mass. This yields the π - d coupling energy $J_{\pi d} \approx g\mu_B H_e/S_{\text{Mn}} < 0.12$ meV (here μ_B is the Bohr magneton and $S_{\text{Mn}} = 5/2$ is the Mn²⁺ spin). This estimation is much smaller than the values $J_{\pi d} \approx 1.5$ and 0.6 meV inferred from the effective internal fields $H_e \approx 32$ and 12.5 T which are reported for λ -(BETS)₂FeCl₄ and κ -(BETS)₂FeBr₄, respectively [9,13,34–36]. The second factor

suppressing the long-range order in the d -electron subsystem is the polymer-type triangular structure of the Mn²⁺ lattice in the anionic layers. The dicyanamide bridges connecting Mn²⁺ ions favor a direct exchange interaction within the anion layers [1], which is likely to prevail the π - d coupling, while the triangular arrangement of Mn²⁺ ions frustrates their AF-type ordering.

V. SUMMARY

The anomalies found in the low-temperature magnetic torque in κ -(BETS)₂Mn[N(CN)₂]₃ have been interpreted in terms of two spatially separated and weakly interacting spin subsystems. One subsystem is associated with d electrons of the Mn²⁺ ions residing in the insulating anion layers, and the other with itinerant π electrons in the conducting molecular layers, which form a long-range AF structure at the Mott-insulating transition. Based on the angular dependence of the high-field torque, the principal axes of magnetization for the Mn²⁺ spin subsystem have been determined. In the insulating state of κ -(BETS)₂Mn[N(CN)₂]₃, the Mn²⁺ magnetization principal axes directions at fields above 10 T are found to be the same as in the metallic state, indicating that the d -electron spin system is totally decoupled from the π spins in this field range. On the other hand, at lower fields a weak interaction between the two subsystems is evidenced by the nonmonotonic behavior of the torque at the field directions near the principal magnetization axes of Mn²⁺. The sharp kink feature observed in the field-dependent torque in a certain angular range is understood as a manifestation of the spin-reorientation transition in the π -electron subsystem. A qualitative analysis of the angular dependence of the kink, involving the Dzyaloshinskii-Moriya interaction in addition to the exchange and Zeeman energy terms, allows us to propose the scheme of the canted AF spin arrangement in this subsystem below and above the spin-reorientation transition.

ACKNOWLEDGMENTS

The authors gratefully acknowledge fruitful discussions with V. Ryazanov and S. Winter. The work was supported by the Deutsche Forschungsgemeinschaft Grant No. KA 1652/4-1 and by the Russian Foundation for Basic Research, Project No. 13-02-00350.

APPENDIX: THE TORQUE CAUSED BY THE SAMPLE GEOMETRY

Consider an isotropic paramagnet in a shape of a general ellipsoid with semiaxes l_a , l_b , and l_c , in the external field \mathbf{H}_e ,

$$\mathbf{H}_e = H_e[\cos\theta, \sin\theta \sin\phi, \sin\theta \cos\phi], \quad (\text{A1})$$

where the polar angle θ and the azimuth angle ϕ are reckoned from l_a and l_b directions, respectively. Once the material is assumed isotropic, the magnetization vector is parallel to \mathbf{H}_e ,

$$\mathbf{M} = M[\cos\theta, \sin\theta \sin\phi, \sin\theta \cos\phi], \quad (\text{A2})$$

and saturates to a constant value at high fields. The demagnetizing field is

$$\mathbf{H}_d = \mu_0 \hat{n} \mathbf{M}, \quad (\text{A3})$$

where the demagnetizing factor

$$\hat{n} = \begin{pmatrix} n_a & 0 & 0 \\ 0 & n_b & 0 \\ 0 & 0 & n_c \end{pmatrix}. \quad (\text{A4})$$

The torque arising from the sample geometry is

$$\begin{aligned} \boldsymbol{\tau}_{\text{dem}} &= V \mathbf{M} \times \mathbf{B} = V \mu_0 \mathbf{M} \times (\mathbf{H}_e - \mathbf{H}_d) \\ &= 2\pi \mu_0 V M^2 [(n_b - n_c) \sin^2 \theta \sin 2\phi, \\ &\quad - (n_a - n_c) \sin 2\theta \cos \phi, (n_a - n_b) \sin 2\theta \sin \phi]. \end{aligned} \quad (\text{A5})$$

The projection of the torque on the field rotation axis, $\mathbf{R} = [0, -\cos \phi, \sin \phi]$, is

$$\begin{aligned} \tau_{\text{dem}}(\theta, \phi) &= \boldsymbol{\tau}_{\text{dem}} \cdot \mathbf{R} = 2\pi \mu_0 V M^2 [(n_a - n_c) \sin 2\theta \cos^2 \phi \\ &\quad + (n_a - n_b) \sin 2\theta \sin^2 \phi]. \end{aligned} \quad (\text{A6})$$

As mentioned in Sec. II, the sample dimensions are 0.08, 0.7, and 0.3 mm along a^* , b , and c crystallographic directions, respectively. Taking these values as the ellipsoid semiaxes, and using the approach of Refs. [37,38] one obtains the demagnetizing factors $n_a = 0.755$, $n_b = 0.057$, and $n_c = 0.188$. For M one can use the maximum value 46.7×10^3 A/m of the saturated paramagnet with $L = 0$, $S = 5/2$, which seems to be a reasonable estimation according to the dc magnetometry data [18]. Then for the rotation axes along $[0\bar{1}0]$ ($\phi = 0$), $[001]$ ($\phi = 90^\circ$), $[0\bar{1}1]$ ($\phi = 55^\circ$), and the perpendicular to $[0\bar{1}1]$ ($\phi = 145^\circ$) Eq. (A6) gives (in units 10^{-7} N m)

$$\tau_{\text{dem}}(\phi = 0^\circ) = 0.13 \sin 2\theta, \quad (\text{A7a})$$

$$\tau_{\text{dem}}(\phi = 90^\circ) = 0.16 \sin 2\theta, \quad (\text{A7b})$$

$$\tau_{\text{dem}}(\phi = 55^\circ) = 0.15 \sin 2\theta, \quad (\text{A7c})$$

$$\tau_{\text{dem}}(\phi = 145^\circ) = 0.14 \sin 2\theta. \quad (\text{A7d})$$

-
- [1] N. D. Kushch, E. B. Yagubskii, M. V. Kartsovnik, L. I. Buravov, A. D. Dubrovskii, A. N. Chekhlov, and W. Biberacher, *J. Am. Chem. Soc.* **130**, 7238 (2008).
- [2] V. N. Zverev, M. V. Kartsovnik, W. Biberacher, S. S. Khasanov, R. P. Shibaeva, L. Ouahab, L. Toupet, N. D. Kushch, E. B. Yagubskii, and E. Canadell, *Phys. Rev. B* **82**, 155123 (2010).
- [3] H. Kobayashi, H. Cui, and A. Kobayashi, *Chem. Rev.* **104**, 5265 (2004).
- [4] H. Kobayashi, H. Tomita, T. Naito, A. Kobayashi, F. Sakai, T. Watanabe, and P. Cassoux, *J. Am. Chem. Soc.* **118**, 368 (1996).
- [5] H. Akutsu, K. Kato, E. Ojima, H. Kobayashi, H. Tanaka, A. Kobayashi, and P. Cassoux, *Phys. Rev. B* **58**, 9294 (1998).
- [6] H. Fujiwara, E. Fujiwara, Y. Nakazawa, B. Zh. Narymbetov, K. Kato, H. Kobayashi, A. Kobayashi, M. Tokumoto, and P. Cassoux, *J. Am. Chem. Soc.* **123**, 306 (2001).
- [7] L. Brossard, R. Clerac, C. Coulon, M. Tokumoto, T. Ziman, D. K. Petrov, V. N. Laukhin, M. J. Naughton, A. Audouard, F. Goze, A. Kobayashi, H. Kobayashi, and P. Cassoux, *Eur. Phys. J. B* **1**, 439 (1998).
- [8] S. Uji, H. Shinagawa, T. Terashima, T. Yakabe, Y. Terai, M. Tokumoto, A. Kobayashi, H. Tanaka, and H. Kobayashi, *Nature (London)* **410**, 908 (2001).
- [9] L. Balicas, J. S. Brooks, K. Storr, S. Uji, M. Tokumoto, H. Tanaka, H. Kobayashi, A. Kobayashi, V. Barzykin, and L. P. Gor'kov, *Phys. Rev. Lett.* **87**, 067002 (2001).
- [10] T. Konoike, S. Uji, T. Terashima, M. Nishimura, S. Yasuzuka, K. Enomoto, H. Fujiwara, E. Fujiwara, B. Zhang, and H. Kobayashi, *Phys. Rev. B* **72**, 094517 (2005).
- [11] T. Konoike, S. Uji, T. Terashima, M. Nishimura, T. Yamaguchi, K. Enomoto, H. Fujiwara, B. Zhang, and H. Kobayashi, *J. Low Temp. Phys.* **142**, 531 (2006).
- [12] M. Kunz, W. Biberacher, N. D. Kushch, A. Miyazaki, and M. V. Kartsovnik, *Phys. Rev. B* **94**, 205104 (2016).
- [13] T. Konoike, S. Uji, T. Terashima, M. Nishimura, S. Yasuzuka, K. Enomoto, H. Fujiwara, B. Zhang, and H. Kobayashi, *Phys. Rev. B* **70**, 094514 (2004).
- [14] H. Fujiwara, H. Kobayashi, E. Fujiwara, and A. Kobayashi, *J. Am. Chem. Soc.* **124**, 6816 (2002).
- [15] M. Kartsovnik, M. Kunz, L. Schaidhammer, F. Kollmannsberger, W. Biberacher, N. Kushch, A. Miyazaki, and H. Fujiwara, *J. Supercond. Nov. Magn.* **29**, 3075 (2016).
- [16] O. M. Vyaselev, M. V. Kartsovnik, N. D. Kushch, and E. B. Yagubskii, *Pisma v Zh. Eksp. Teor. Fiz.* **95**, 961 (2012) [*JETP Lett.* **95**, 565 (2012)].
- [17] O. M. Vyaselev, R. Kato, H. M. Yamamoto, M. Kobayashi, L. V. Zorina, S. V. Simonov, N. D. Kushch, and E. B. Yagubskii, *Crystals* **2**, 224 (2012).
- [18] O. M. Vyaselev, M. V. Kartsovnik, W. Biberacher, L. V. Zorina, N. D. Kushch, and E. B. Yagubskii, *Phys. Rev. B* **83**, 094425 (2011).
- [19] O. M. Vyaselev, N. D. Kushch, and E. B. Yagubskii, *Zh. Eksp. Teor. Fiz.* **140**, 961 (2011) [*JETP* **113**, 835 (2011)].
- [20] P. Christ, W. Biberacher, H. Müller, and K. Andres, *Solid State Commun.* **91**, 451 (1994).
- [21] M. Pinterić, M. Miljak, N. Biškup, O. Milat, I. Aviani, S. Tomić, D. Schweitzer, W. Strunz, and I. Heinen, *Eur. Phys. J. B* **11**, 217 (1999).
- [22] A. Cornia, D. Gatteschi, and R. Sessoli, *Coord. Chem. Rev.* **219–221**, 573 (2001).
- [23] D. F. Smith, S. M. De Soto, C. P. Slichter, J. A. Schlueter, A. M. Kini, and R. G. Daugherty, *Phys. Rev. B* **68**, 024512 (2003).
- [24] D. F. Smith, C. P. Slichter, J. A. Schlueter, A. M. Kini, and R. G. Daugherty, *Phys. Rev. Lett.* **93**, 167002 (2004).
- [25] I. E. Dzialoshinskii, *Zh. Eksp. Teor. Fiz. (U.S.S.R.)* **32**, 1547 (1957) [*Sov. Phys. JETP* **5**, 1259 (1957)].
- [26] T. Moriya, *Phys. Rev.* **120**, 91 (1960).
- [27] U. Welp, S. Fleshler, W. K. Kwok, G. W. Crabtree, K. D. Carlson, H. H. Wang, U. Geiser, J. M. Williams, and V. M. Hitsman, *Physica B* **186–188**, 1065 (1993).
- [28] S. M. Winter, S. Hill, and R. T. Oakley, *J. Am. Chem. Soc.* **137**, 3720 (2015).
- [29] O. M. Vyaselev *et al.* (unpublished).
- [30] T. Konoike, S. Uji, M. Nishimura, K. Enomoto, H. Fujiwara, B. Zhang, and H. Kobayashi, *Physica B* **359–361**, 457 (2005).

- [31] M. Tokumoto, H. Tanaka, T. Otsuka, H. Kobayashi, and A. Kobayashi, *Polyhedron* **24**, 2793 (2005).
- [32] M. V. Kartsovnik, V. N. Zverev, W. Biberacher, S. V. Simonov, I. Sheikin, N. D. Kushch, and E. B. Yagubskii, *Low Temp. Phys.* **43**, 239 (2017).
- [33] D. Shoenberg, *Magnetic Oscillations in Metals* (Cambridge University Press, Cambridge, 1984).
- [34] O. Cépas, R. H. McKenzie, and J. Merino, *Phys. Rev. B* **65**, 100502 (2002).
- [35] K. Hiraki, H. Mayaffre, M. Horvatić, C. Berthier, S. Uji, T. Yamaguchi, H. Tanaka, A. Kobayashi, H. Kobayashi, and T. Takahashi, *J. Phys. Soc. Jpn.* **76**, 124708 (2007).
- [36] S. Fujiyama, M. Takigawa, J. Kikuchi, H.-B. Cui, H. Fujiwara, and H. Kobayashi, *Phys. Rev. Lett.* **96**, 217001 (2006).
- [37] J. A. Osborn, *Phys. Rev.* **67**, 351 (1945).
- [38] M. Beleggia, M. De Graef, and Y. Millev, *Philos. Mag.* **86**, 2451 (2006).